nature geoscience

ARTICLES

PUBLISHED ONLINE: 19 JANUARY 2014 | DOI: 10.1038/NGEO2062

Mantle flow and multistage melting beneath the Galápagos hotspot revealed by seismic imaging

Darwin R. Villagómez[1†], Douglas R. Toomey[1*], Dennis J. Geist[2], Emilie E. E. Hooft[1] and Sean C. Solomon[3]

Some of Earth's largest magmatic provinces result from the interaction between mid-ocean ridges and near-ridge hotspots, which are hypothesized to overlie plumes of upwelling mantle. Geodynamic models predict that upwelling plumes are sheared by the motion of the overlying tectonic plates and can connect to a nearby mid-ocean ridge by shallow flow beneath thin, young lithosphere. Here we present seismic tomographic images of the upper 300 km of the mantle beneath the Galápagos Archipelago in the eastern Pacific Ocean. We observe a low-velocity anomaly, indicative of an upwelling plume, that is not deflected in the direction of plate motion. Instead, the anomaly tilts towards the mid-ocean ridge at depths well below the lithosphere. These characteristics of the plume–ridge connection beneath the Galápagos Archipelago are consistent with the presence of multiple stages of partial melting, melt extraction, and melt remixing within the plume and surrounding mantle. These processes affect the viscosity of the asthenosphere, alter the upwelling plume and influence the compositions of surface lavas. Our results imply that the coupling between the oceanic plate and plume upwelling beneath the Galápagos is weak. Multistage melting may similarly affect the geophysical and geochemical characteristics of other hotspots.

Most previous seismic studies of hotspots have focused on their deeper structure to test the mantle plume hypothesis[1]. Such studies have provided a wealth of information about convection in Earth's mantle, including the depth, geometry, and physical properties of mantle plumes[2–5]. Mantle convection models predict that plumes are deflected at shallow depths by the motion of the overlying plate[6]. Moreover, material upwelling in a plume near a mid-ocean ridge is predicted to flow towards the spreading axis along the base of the cooling lithosphere[1,7,8]. Despite the importance of such models for understanding magmatism and for deducing the dynamics of the upper mantle[9], there have heretofore been no high-resolution images of mantle structure beneath a near-ridge hotspot. Tomographic images of the mantle beneath the Galápagos Archipelago provide critical evidence for the nature of plume–lithosphere–ridge interactions as well as for the extent of viscous coupling between oceanic plates and the asthenosphere. Both of these issues are of global importance for understanding plate motions and return flow from the deep mantle to spreading centres.

Geologic setting of the Galápagos

The Galápagos hotspot–ridge system consists of the Galápagos Archipelago, which marks the current location of the volcanic hotspot, and the Galápagos Spreading Center (GSC), which is located 100–200 km to the north of the archipelago and has a complicated history of migration with respect to the hotspot[10,11] (Fig. 1). The archipelago sits on the Nazca plate, which moves eastwards with respect to a hotspot reference frame[12]. The GSC has a half-spreading rate of 28 mm yr^{-1} in a north–south direction[10], a direction approximately perpendicular to the motion of the Nazca plate over the hotspot. In addition to the volcanoes that lie on the main hotspot trace, five islands and dozens of seamounts lie between the central archipelago and the GSC, and their origin has been attributed to the flow of plume material towards the spreading centre[11,13,14].

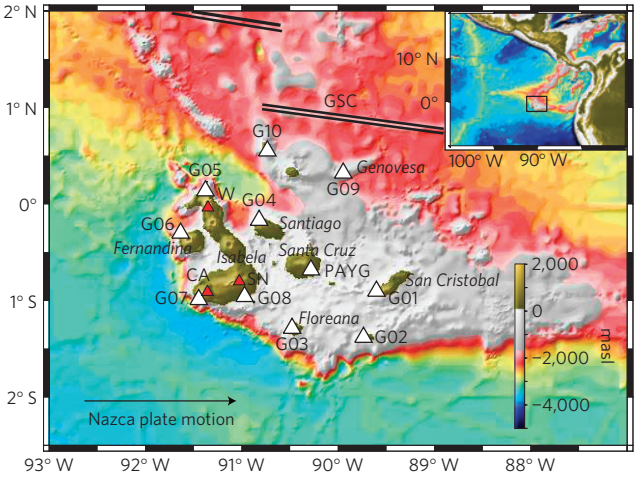

Figure 1 | Map of the Galápagos Islands and seismic network. Triangles indicate seismic stations; the network consisted of ten portable broadband stations and the Global Seismographic Network (GSN) station PAYG. Selected islands and volcanoes are labelled in italics and red, respectively (SN, Sierra Negra; CA, Cerro Azul; W, Wolf). The black arrow indicates the direction of motion of the Nazca plate in a hotspot reference frame[12]. Bathymetry and topography in metres above sea level (masl). Inset shows the location in a broader context.

The GSC shows evidence of interaction with the hotspot for more than 1,000 km along its length (~85°–96° W). There are anomalies in elevation, crustal thickness, gravity field, ridge morphology, trace element concentrations, radiogenic isotope

[1]Department of Geological Sciences, University of Oregon, Eugene, Oregon 97403, USA, [2]Department of Geological Sciences, University of Idaho, Moscow, Idaho 83844, USA, [3]Lamont-Doherty Earth Observatory, Columbia University, Palisades, New York 10964, USA. [†]Present address: ID Analytics, San Diego, California 92128, USA. *e-mail: drt@uoregon.edu

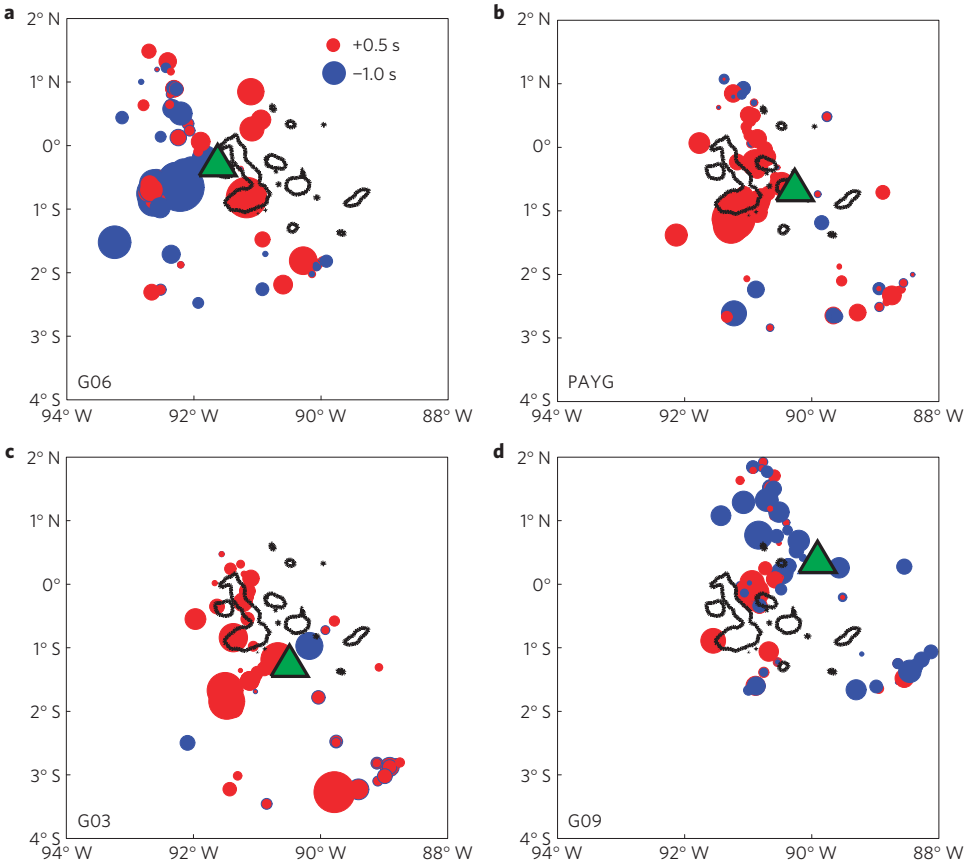

Figure 2 | Delay times of teleseismic S waves. Each delay time (circle) is plotted at the piercing point where the seismic wave path to a given station (triangle) intersects a horizontal plane at 300 km depth. Delay times have been adjusted by station corrections (see Supplementary Information). Red and blue circles indicate positive (late) and negative (early) delays, respectively. The size of the symbol is proportional to the observed delay, as indicated by the scale at the top right in **a**. **a**, Station G06, located on Fernandina. **b**, GSN station PAYG, located on Santa Cruz. **c**, Station G03, located on Floreana. **d**, Station G09, located on Genovesa.

compositions, and volatile abundances that are generally centred about 91° W and decrease in amplitude to the east and west[15–21].

Seismic experiment and tomographic imaging

Between September 1999 and March 2003 we deployed ten portable broadband stations on islands of the Galápagos Archipelago (Fig. 1). That experiment has already provided information on the structure of the crust, the structure of the mantle to depths of ~125 km, and the thickness of the mantle transition zone[22–24]. Here we combine our previous observations of Rayleigh wave phase velocities with new observations of teleseismic S wave delay times to constrain mantle structure to depths of 300 km.

Examples of S wave delay times at four stations, shown in Fig. 2, provide a simple means for assessing regions of anomalous mantle structure (see Supplementary Methods). Observations from the island of Fernandina (Fig. 2a), the most active and westernmost volcano in the archipelago, show that S waves arriving from the west are anomalously early, indicating above-average mantle velocities in this region. Early arrivals are also consistently observed from paths that pass only beneath the northern portion of the archipelago and the GSC (Fig. 2d). Generally, S waves that traverse the mantle beneath the island of Isabela (91°–92° W) arrive anomalously late, with the largest delays observed for paths from the south (Fig. 2b,c). These results indicate that depth-averaged seismic velocities are lower than average beneath the southern end of Isabela and higher beneath and to the west of Fernandina.

The results of tomographic inversion (see Supplementary Methods) for the S-wave velocity (V_S) reveal anomalously low seismic velocities in several distinct regions (Fig. 3). First, near southern Isabela, low velocities extend from the shallow mantle to depths of at least 300 km. A north–south section at 91° W shows the low-velocity anomaly to be continuous (Fig. 3e), and between 300 and 100 km it tilts northwards at an angle of ~45° as it shoals. An east–west section through the low-velocity anomaly at 0° 45′ S (Fig. 3d) reveals a columnar feature that is ~100 km wide and continuous from ~100 to 300 km depth. The top of this low-velocity anomaly is overlain by a zone in which V_S is higher than normal at depths from 80 to 150 km (Fig. 3d,e).

At depths shallower than 100–150 km, two distinct volumes of low velocities are observed. The first is a larger-magnitude low-velocity anomaly (maximum V_S anomaly of −2%) centred near 50 km depth and located beneath the southwestern part of the archipelago (Fig. 3a). This anomaly is resolved primarily by the surface wave data, and its lateral extent is ~200 km in the east–west direction and ~100 km in the north–south direction. The spatial extent of this anomaly is well constrained within the seismic array, but it is less well constrained to the southwest because of the lack of stations in that region. In map view the anomaly overlaps the region of lower velocities observed at depths greater than 100 km but is offset to the northwest. A second volume of relatively low seismic velocities is observed beneath the northeastern archipelago at depths of 50–150 km (Fig. 3b). Within the seismic array the lateral dimensions and depth extent of the anomaly are well constrained. However, north of ~1° N, towards the GSC, the extent of the anomaly is poorly constrained[22].

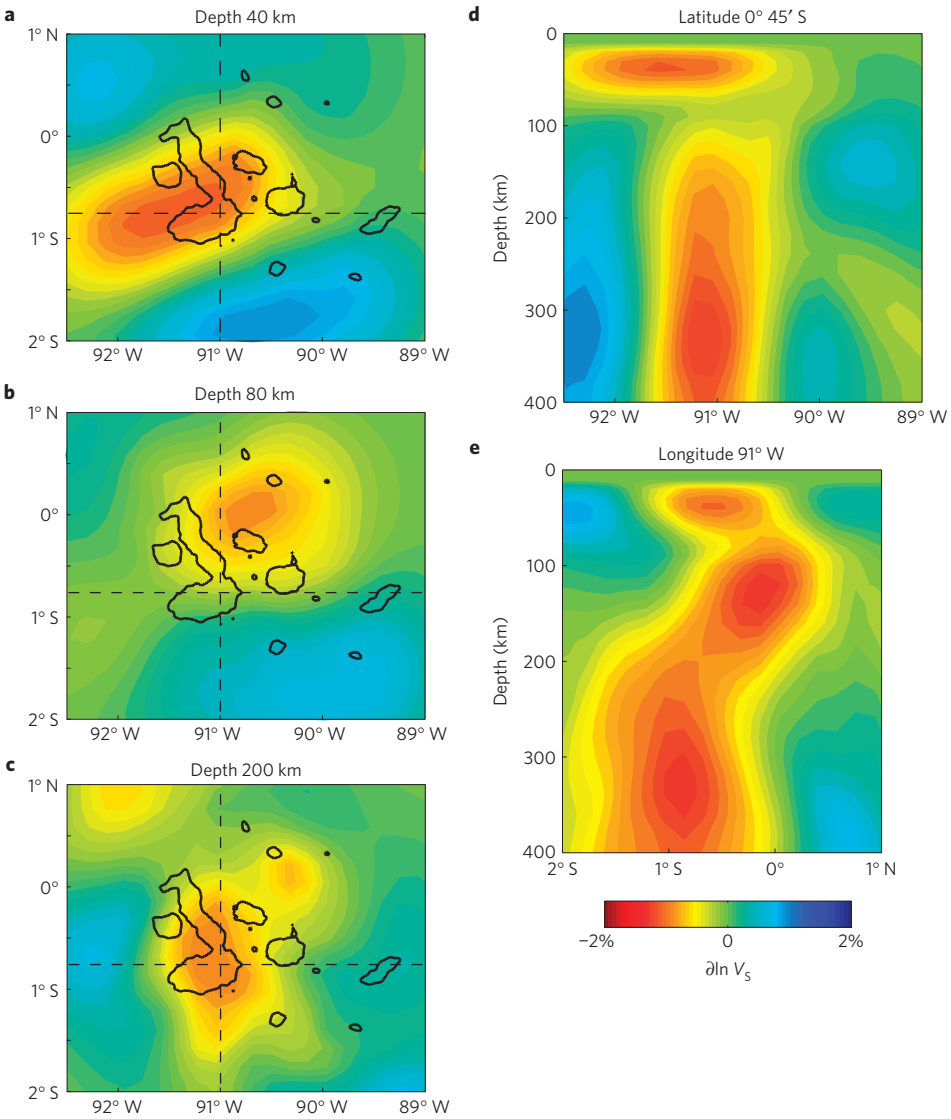

Figure 3 | Results of tomographic inversion for S-wave velocity structure. Colour scale denotes the percentage deviation from the starting model (see Fig. 11 of ref. 22). **a**–**c**, Map-view horizontal section at 40 km depth (**a**), 80 km depth (**b**), and 200 km depth (**c**). **d**, East–west cross-section at 0°45′ S. **e**, North–south cross-section at 91° W. Dashed lines in **a**–**c** indicate locations of cross-sections **d**,**e**.

Two volumes of relatively high seismic velocities are notable. The first is an anomaly with velocities at least 1% greater than average that extends to depths of 100–150 km, with the greater depths beneath southern Isabela (Fig. 3d,e); see Supplementary Fig. 2 for resolution tests. This high-velocity lid was noted from surface-wave analysis and has been attributed to the depleted and dehydrated residuum remaining after partial melt extraction[22]. A second high-velocity anomaly, which is well expressed in the delay time data (Fig. 2a) but poorly imaged, is located immediately to the west of Fernandina (Fig. 3c,d). Given the magnitude of the delays west of Fernandina, which are the largest observed, it is not possible that the anomalous velocities are restricted to the lithosphere or to depths less than 100 km (see Supplementary Information). Although we cannot constrain the geometry and depth extent of this feature with the data available at present, we can determine with confidence that velocities are generally higher than average in the sublithospheric mantle west of the archipelago.

Plume ascent in the Galápagos

We attribute regions of anomalously low seismic velocities to thermal anomalies and melting associated with the Galápagos mantle plume, and we emphasize three aspects of the plume's ascent: the upwelling plume is not centred beneath Fernandina, which is usually considered the leading edge of the Galápagos hotspot[25]; the plume is deflected or bent towards the GSC, but not in the direction of plate motion, and this bending occurs at depths (>150 km) much greater than the base of the thermal lithosphere; and at relatively shallow depths (~50 km) the Galápagos seismic anomaly extends 'upstream' from Fernandina, that is, opposite to the direction of plate motion, well to the west of the westernmost island.

Most models of plume–lithosphere interaction that include viscous coupling between plate motion and plume upwelling predict deflection of a plume in the direction of plate motion[6]. Fernandina, with its high $^3He/^4He$ anomaly and its westernmost position within the archipelago, should thus overlie the locus of plume upwelling. However, the Galápagos plume at 250 km depth is centred well to the east and south of the western edge of the hotspot. The locus of plume upwelling, therefore, cannot be accurately determined from surface geology, geochemistry, and plate motions.

As the Galápagos plume shoals from 250 to 100 km depth, it tilts northwards towards the GSC, in a direction approximately

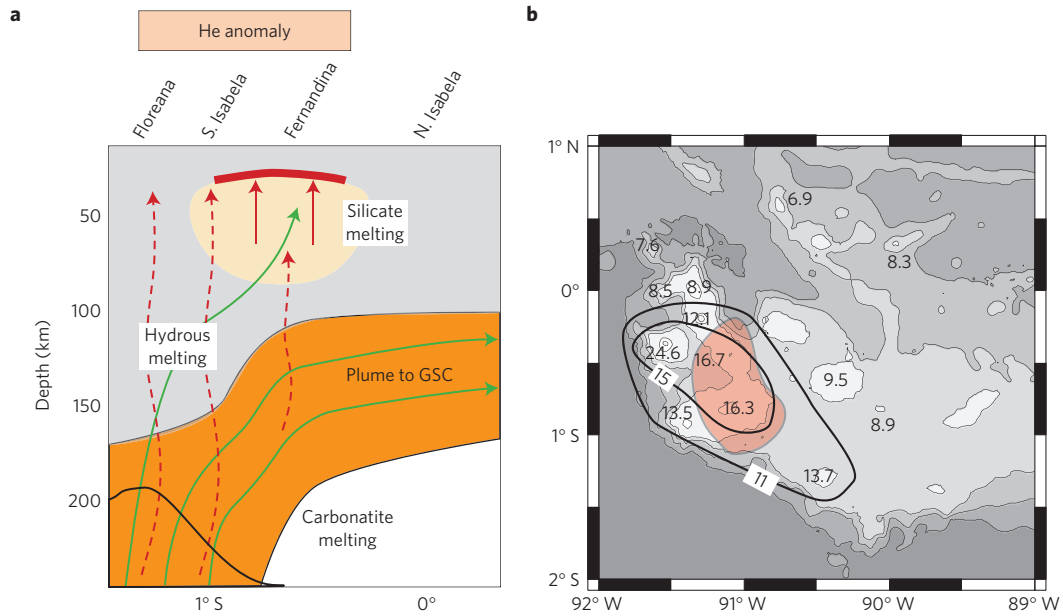

Figure 4 | Schematic illustration of mantle flow and melting and their relation to geochemical observations. a, North–south cross-section at 91° W, perpendicular to the plate motion. Also indicated are the mantle flow direction (green); ascent of carbonated and hydrous melts (dashed red arrows); ascent of silicate melts (solid red arrows); zone of melt mixing (thick red line); enriched plume (orange); dehydrated volume (grey); and zone of elevated temperature and water content within the plume (black curve). The latitudinal extent of the He anomaly is indicated by the box above the map. **b**, Map of $^{3}He/^{4}He$ ratios and anomalous seismic velocities at 200 km depth (coloured region denotes shear velocities at least 0.75% lower than average). Helium data compiled from the GEOROC database. Numbers are average values for individual volcanoes; $^{3}He/^{4}He$ contoured at values of 11 and 15.

perpendicular to plate motion, and is overlain by a high-velocity lid at 100–150 km depth (Fig. 3e). This high-velocity lid is attributed to olivine dehydration[22,24], which increases seismic velocities and viscosity[26], thereby decreasing the upward flow rate. The high-velocity lid is thickest beneath southern Isabela and above the columnar low-velocity anomaly imaged at depths greater than 150 km. The plume is deflected towards the GSC at depths well below the base of the thermal lithosphere, which is at a depth less than 50 km, given the plate age. Parallel to plate motion (Fig. 3d), the plume is a vertical feature centred on 91° W, the same longitude as the peak in the geochemical and geophysical anomalies along the GSC (ref. 19). In order for the plume to ascend from 250 km with no deflection by plate motion, either plume buoyancy must be much greater than predicted by geodynamic models, or the plume must not be viscously coupled to the motion of the Nazca plate[6].

The low-velocity anomaly of greatest magnitude is found between the base of the crust and 80 km depth and underlies the three most active volcanoes in the archipelago: Sierra Negra, Cerro Azul, and Fernandina (Fig. 3a). The vertical extent of this anomaly is consistent with decompression melting of anhydrous peridotite, indicating that the anomaly may mark a volume of partial melting that feeds volcanism. The seismic anomaly is constrained primarily by surface wave data, which require that it extend well to the west of any volcanoes[22]. Two complementary mechanisms could drive upwelling in this region. First, the buoyancy of the plume could drive dehydrated residuum upwards. Second, the upwelling may also be a response to downwelling along the margins of the archipelago, as indicated by the higher than average seismic velocities to the west and by numerical models for plume dynamics and seismic observations of the mantle beneath the Hawaiian hotspot[4,27].

Multistage melting in a volatile-bearing mantle

Our tomographic results provide a view of the internal structure of an ascending plume that is consistent with multiple stages of melting of volatile-bearing peridotite. Three vertical zones are defined by changes in seismic velocities with depth, and we attribute these zones to three stages of melting (Fig. 4a): a deep (>150 km), low-velocity zone in which incipient carbonatite or carbonate-rich silicate melt is produced; an intermediate-depth (150–80 km) high-velocity zone in which hydrogen is removed from olivine; and a shallow (<80 km depth) low-velocity zone in which silicate minerals undergo greater extents of melting. Although the buoyant melts derived from the three regions might initially rise separately, our hypothesis is that, because the three melting zones are vertically aligned, the melts mix before their intrusion into the lithosphere and eventual eruption.

The carbonated-melting zone. Melting of carbonated peridotite, in conjunction with elevated temperatures and hydrogen concentrations, is consistent with the deep columnar low-velocity anomalies at >150 km depth. Small amounts of carbonate-rich melt are produced by the upwelling of carbonated peridotite[28,29]. The greatest depth at which the solidus temperature is reached depends on the temperature and redox state of the mantle and thus is uncertain[29,30]. We predict initiation of melting at 300–400 km, given what is known about the mantle's oxygen fugacity, carbon concentrations, and excess potential temperatures of 40–100 K (refs 28,29). In support of this interpretation, we note that $^{3}He/^{4}He$ ratios are elevated in lavas of the southwestern volcanoes of the archipelago (Fig. 4b), a region that overlies the zone of low seismic velocities at 200–250 km. We attribute this correlation to deep melting, with subsequent extraction and vertical transport of melt having elevated $^{3}He/^{4}He$ ratios.

The hydrogen-extraction zone. The high-velocity lid (150–80 km depth beneath southern Isabela) has seismic velocities 1–2% greater than velocities below. The solidus of garnet lherzolite with 250–800 ppm H_2O is ~40–80 km deeper than that for anhydrous garnet lherzolite[31], values consistent with the variable depth of the high-velocity lid. The removal of hydrogen from olivine increases

seismic velocities[32] and viscosity, the latter by about two orders of magnitude[26]. We attribute the intermediate zone of relatively high seismic velocities to dehydration of olivine by small degrees of partial melting[22,33]. Several studies have indicated that the Galápagos plume is zoned, with a greater concentration of primitive and recycled material in the southwest[34,35]. In combination with greater temperatures in this part of the mantle, the dehydrated region is thickest in the southwestern archipelago (Fig. 4a).

The silicate-melting zone. The uppermost low-velocity zone beneath the volcanically active western Galápagos extends downwards from near the base of the crust to approximately 80 km depth. The seismic anomalies are about 2% lower than average, a value that is consistent with a small amount (1%) of silicate melt retained in the mantle[22]. The vertical extent of the anomaly is consistent with evidence from trace element abundances that western Galápagos magmas are extracted from source regions that contain garnet[36–38].

A new hypothesis for plume–ridge interaction

Models of two-way exchange of material between a deeply rooted mantle plume and the upper mantle can account for most of the geochemical anomalies of the Galápagos Islands and the nearby GSC (refs 15,34,39). Two paradoxes, however, defy simple models. First, there are pronounced anomalies in the Sr, Nd, Pb and Hf isotopic ratios along the GSC (refs 15,19,20), but there is no $^3He/^4He$ anomaly, despite the fact that the Galápagos Islands are a high $^3He/^4He$ hotspot[25,40,41]. Second, volcanoes from both the central Galápagos Platform and many of the islands and seamounts between the platform and the GSC (refs 14,34; for example, Genovesa Island) are more depleted isotopically than any GSC lavas within ~400 km of 91° W (ref. 19). In other words, the GSC has more plume-like compositions than much of the hotspot province.

To reconcile these paradoxes, we call on the separate transport of carbonate-rich melts produced by deep melting and carbon-depleted residuum towards the GSC. It has been proposed that helium is transported by carbonatite melt in the Hawaiian plume and that such melt moves separately from the plume flow[42]. In the Galápagos, the plume is not deflected by plate motion, so the carbonatite melt should flow vertically with the upwelling mantle that partially melts again at shallower depths (Fig. 4a). The carbonatite melt and dissolved helium are therefore cryptic, because they mix with the more shallowly produced silicate melts.

A 0.1% carbonatite (or carbonate-rich silicate) melt of depleted mantle has a strongly incompatible-element-enriched composition (Fig. 5) and, when mixed with a 5% melt of garnet lherzolite, the hybrid has a trace element pattern very similar to that of the basalts of Fernandina. The key aspect of this hypothesis is that helium is transported with the carbonatite melts, but Sr, Nd, Pb, Hf, and water are mostly retained in the carbon-depleted residuum (Fig. 4a).

We also hypothesize that mixing of melts from carbonatite-depleted peridotite and the ambient upper mantle can account for the isotopic and elemental differences between the Galápagos Islands and the GSC. Because the GSC has an H_2O anomaly at 91° W (ref. 18), we infer that transport of plume material towards the GSC occurs at depths greater than the hydrous solidus (>100 km), an interpretation consistent with the low velocities imaged seismically (Fig. 3e). Therefore, we propose that plume material is carried to the GSC by relatively deep asthenospheric 'return flow', rather than flow along the base of the lithosphere, as in most models of plume–ridge interaction (for example, those of ref. 9 and cited therein).

Transport of material towards the GSC in the deep asthenosphere may also account for the depleted compositions of lavas from many of the northern and central Galápagos volcanoes compared with nearby GSC lavas[39]. In the standard model, by which plume material flows towards the GSC at the base of the lithosphere, the geochemical signal of plume contribution should decrease radially away from the plume. The depleted magmas of the northern Galápagos, in contrast, may be produced by remelting of material that was already melted at the GSC, where most of the material with enriched Sr, Nd, Pb and Hf isotopic compositions was removed because of its lower solidus temperature. The twice-depleted material is transported away from the GSC beneath newly formed oceanic lithosphere and then melts in response to local extension[14]. A possibility that need not replace the above scenario is that the depleted magmas observed in the central and northern Galápagos may result from geochemical zonation in the upwelling plume[34,35,43,44].

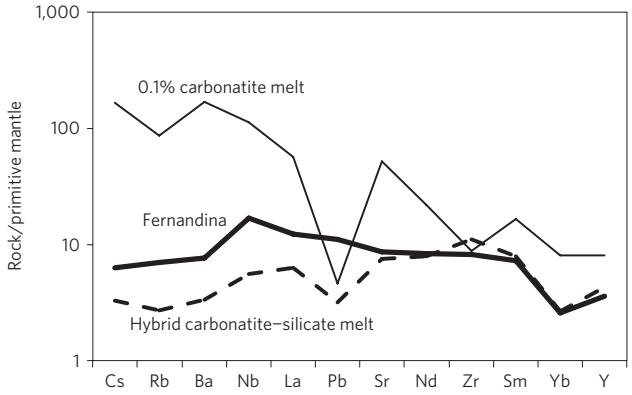

Figure 5 | Predicted and observed trace element compositions of magmas produced by melting of the Galápagos plume. A 0.1% carbonatite melt (thin line) and a calculated hybrid of that melt and a 5% silicate melt of the residue (dashed line) are compared with a basalt sample from Fernandina (thick line). The source is assumed to have 20% clinopyroxene and 10% garnet. Carbonatite–liquid distribution coefficients are from ref. 30. The Fernandina basalt composition[48] has been corrected for 50% fractional crystallization. The source composition is depleted MORB (mid-ocean ridge basalt) mantle[49]. Concentrations are normalized to the primitive mantle composition[50].

We conclude that models involving entrainment of depleted upper mantle into an eastward-tilting mantle plume[36,39,45] or ponding of plume material beneath young, thin lithosphere[7,8,46] are not supported by our results. Instead, the connection between the hotspot and the ridge occurs in the deeper asthenosphere, and transport of plume material to the ridge is poorly coupled to plate motion. Multistage melting is the main arbiter of seismic velocities, mantle viscosity, the three-dimensional flow of plume material, and the resulting petrological and geochemical anomalies observed in the Galápagos Archipelago and along the GSC. Seismic models of the mantle beneath other hotspot provinces[4] may match similar scenarios involving formation of a deep incipient carbonatite melt and the effects of dehydration melting.

Methods

Seismic analysis. We measured 1,769 S-wave relative delay times from 161 teleseismic events (body wave magnitude $m_b > 5.5$) with respect to a standard Earth model (see Supplementary Information). Because body waves and surface waves provide complementary information on seismic velocity structure, we simultaneously inverted observations of shear wave delay times and Rayleigh wave phase velocities for mantle structure. To do so we modified previous methods[47] to develop a nonlinear algorithm that includes variable weighting of body and surface wave data and three-dimensional seismic ray tracing (see Supplementary Information for details). Synthetic tests indicate that our methodology is superior to separate inversions of surface or body wave data (Supplementary Fig. 2).

Received 14 August 2013; accepted 9 December 2013; published online 19 January 2014

References

1. Morgan, W. J. Convection plumes in the lower mantle. *Nature* **230,** 42–43 (1971).

2. Wolfe, C. J., Bjarnason, I. T., VanDecar, J. C. & Solomon, S. C. Seismic structure of the Iceland mantle plume. *Nature* **385,** 245–247 (1997).
3. Montelli, R. *et al.* Finite-frequency tomography reveals a variety of plumes in the mantle. *Science* **303,** 338–343 (2004).
4. Wolfe, C. J. *et al.* Mantle shear-wave velocity structure beneath the Hawaiian hot spot. *Science* **326,** 1388–1390 (2009).
5. Schmandt, B., Dueker, K., Humphreys, E. & Hansen, S. Hot mantle upwelling across the 660 beneath Yellowstone. *Earth Planet. Sci. Lett.* **331–332,** 224–236 (2012).
6. Ribe, N. M. & Christensen, U. R. Three-dimensional modeling of plume–lithosphere interaction. *J. Geophys. Res.* **99,** 669–682 (1994).
7. Ribe, N. M. The dynamics of plume–ridge interaction 2. Off-ridge plumes. *J. Geophys. Res.* **101,** 16195–16204 (1996).
8. Feighner, M. A. & Richards, M. A. The fluid dynamics of plume–ridge and plume-plate interactions: An experimental investigation. *Earth Planet. Sci. Lett.* **129,** 171–182 (1995).
9. Ito, G., Lin, J. & Graham, D. Observational and theoretical studies of the dynamics of mantle plume–mid-ocean ridge interaction. *Rev. Geophys.* **41,** 1017 (2003).
10. Wilson, D. S. & Hey, R. N. History of rift propagation and magnetization intensity for the Cocos-Nazca spreading center. *J. Geophys. Res.* **100,** 10041–10056 (1995).
11. Mittelstaedt, E. *et al.* Multiple expressions of plume–ridge interaction in the Galápagos: Volcanic lineaments and ridge jumps. *Geochem. Geophys. Geosyst.* **13,** Q05018 (2012).
12. Gripp, A. E. & Gordon, R. G. Young tracks of hotspots and current plate velocities. *Geophys. J. Int.* **150,** 321–361 (2002).
13. Morgan, W. J. Rodriguez, Darwin, Amsterdam,..., a second type of hotspot island. *J. Geophys. Res.* **83,** 5355–5360 (1978).
14. Harpp, K. & Geist, D. Wolf-Darwin lineament and plume–ridge interaction in northern Galápagos. *Geochem. Geophys. Geosyst.* **3,** 8504 (2002).
15. Schilling, J. G., Kingsley, R. H. & Devine, J. D. Galapagos hot spot-spreading center system 1. Spatial petrological and geochemical variations (83° W–111 °W). *J. Geophys. Res.* **87,** 5593–5610 (1982).
16. Ito, G. T. & Lin, J. Mantle temperature anomalies along the past and paleoaxes of the Galápagos spreading center as inferred from gravity analyses. *J. Geophys. Res.* **100,** 3733–3745 (1995).
17. Canales, J. P., Ito, G., Detrick, R. S. & Sinton, J. Crustal thickness along the western Galapagos Spreading Center and the compensation of the Galapagos hotspot swell. *Earth Planet. Sci. Lett.* **203,** 311–327 (2002).
18. Detrick, R. S. *et al.* Correlated geophysical, geochemical, and volcanological manifestations of plume–ridge interaction along the Galápagos Spreading Center. *Geochem. Geophys. Geosyst.* **3,** 8501 (2002).
19. Schilling, J., Fontignie, D., Blichert-Toft, J., Kingsley, R. & Tomza, U. Pb–Hf–Nd–Sr isotope variations along the Galápagos Spreading Center (101–83 W): Constraints on the dispersal of the Galápagos mantle plume. *Geochem. Geophys. Geosyst.* **4,** 8512 (2003).
20. Ingle, S. *et al.* Mechanisms of geochemical and geophysical variations along the western Galápagos Spreading Center. *Geochem. Geophys. Geosyst.* **11,** Q04003 (2010).
21. Shorttle, O., Maclennan, J. & Jones, S. M. Control of the symmetry of plume–ridge interaction by spreading ridge geometry. *Geochem. Geophys. Geosyst.* **11,** Q0AC05 (2010).
22. Villagómez, D., Toomey, D. R., Hooft, E. E. E. & Solomon, S. C. Upper mantle structure beneath the Galápagos Archipelago from surface wave tomography. *J. Geophys. Res.* **112,** B07303 (2007).
23. Hooft, E. E. E., Toomey, D. R. & Solomon, S. C. Anomalously thin transition zone beneath the Galápagos hotspot. *Earth Planet. Sci. Lett.* **216,** 55–64 (2003).
24. Villagómez, D. R., Toomey, D. R., Hooft, E. E. E. & Solomon, S. C. Crustal structure beneath the Galápagos Archipelago from ambient noise tomography and its implications for plume–lithosphere interactions. *J. Geophys. Res.* **116,** B04310 (2011).
25. Kurz, M. D. & Geist, D. Dynamics of the Galapagos hotspot from helium isotope geochemistry. *Geochim. Cosmochim. Acta* **63,** 4139–4156 (1999).
26. Hirth, G. & Kohlstedt, D. L. Water in the oceanic upper mantle: implications for rheology, melt extraction and the evolution of the lithosphere. *Earth Planet. Sci. Lett.* **144,** 93–108 (1996).
27. Moore, W. B., Schubert, G. & Tackley, P. Three-dimensional simulations of plume–lithosphere interaction at the Hawaiian Swell. *Science* **279,** 1008–1011 (1998).
28. Dasgupta, R. & Hirschmann, M. M. Melting in the Earth's deep upper mantle caused by carbon dioxide. *Nature* **440,** 659–662 (2006).
29. Dasgupta, R. *et al.* Carbon-dioxide-rich silicate melt in the Earth's upper mantle. *Nature* **493,** 211–215 (2013).
30. Dasgupta, R., Hirschmann, M. M., McDonough, W. F., Spiegelman, M. & Withers, A. C. Trace element partitioning between garnet lherzolite and carbonatite at 6.6 and 8.6 GPa with applications to the geochemistry of the mantle and of mantle-derived melts. *Chem. Geol.* **262,** 57–77 (2009).
31. Hirschmann, M. M. Water, melting, and the deep Earth H_2O cycle. *Annu. Rev. Earth. Planet. Sci.* **34,** 629–653 (2006).
32. Karato, S-I. Remote sensing of hydrogen in Earth's mantle. *Rev. Mineral. Geochem.* **62,** 343–375 (2006).
33. Hall, P. S. & Kincaid, C. Melting, dehydration, and the dynamics of off-axis plume–ridge interaction. *Geochem. Geophys. Geosyst.* **4,** 8510 (2003).
34. Harpp, K. S. & White, W. M. Tracing a mantle plume: Isotopic and trace element variations of Galápagos seamounts. *Geochem. Geophys. Geosyst.* **2,** 1042 (2001).
35. Hoernle, K. *et al.* Existence of complex spatial zonation in the Galápagos plume. *Geology* **28,** 435–438 (2000).
36. White, W. M., McBirney, A. R. & Duncan, R. A. Petrology and geochemistry of the Galápagos Islands: Portrait of a pathological mantle plume. *J. Geophys. Res.* **98,** 19533–19563 (1993).
37. Geist, D. *et al.* Wolf Volcano, Galapagos Archipelago: Melting and magmatic evolution at the margins of a mantle plume. *J. Petrol.* **46,** 2197–2224 (2005).
38. Gibson, S. A. & Geist, D. Geochemical and geophysical estimates of lithospheric thickness variation beneath Galápagos. *Earth Planet. Sci. Lett.* **300,** 275–286 (2010).
39. Geist, D. J., White, W. M. & McBirney, A. R. Plume-asthenosphere mixing beneath the Galapagos archipelago. *Nature* **333,** 657–660 (1988).
40. Graham, D. W., Christie, D. M. & Harpp, K. S. Mantle plume helium in submarine basalts from the Galápagos platform. *Science* **262,** 2023–2026 (1993).
41. Colin, A., Burnard, P. G., Graham, D. W. & Marrocchi, Y. Plume-ridge interaction along the Galapagos Spreading Center: Discerning between gas loss and source effects using neon isotopic compositions and ^4He–^{40}Ar–CO_2 relative abundances. *Geochim. Cosmochim. Acta* **75,** 1145–1160 (2011).
42. Hofmann, A. W., Farnetani, C. G., Spiegelman, M. & Class, C. Displaced helium and carbon in the Hawaiian plume. *Earth Planet. Sci. Lett.* **312,** 226–236 (2011).
43. Weis, D., Garcia, M. O., Rhodes, J. M., Jellinek, M. & Scoates, J. S. Role of the deep mantle in generating the compositional asymmetry of the Hawaiian mantle plume. *Nature Geosci.* **4,** 831–838 (2011).
44. Huang, S., Hall, P. S. & Jackson, M. G. Geochemical zoning of volcanic chains associated with Pacific hotspots. *Nature Geosci.* **4,** 874–878 (2011).
45. Richards, M. A. & Griffiths, R. W. Thermal entrainment by deflected mantle plumes. *Nature* **342,** 900–902 (1989).
46. Ito, G., Lin, J. & Gable, C. W. Interaction of mantle plumes and migrating mid-ocean ridges: Implications for the Galápagos plume–ridge system. *J. Geophys. Res.* **102,** 15403–15417 (1997).
47. Hammond, W. C. & Toomey, D. R. Seismic velocity anisotropy and heterogeneity beneath the Mantle Electromagnetic and Tomography Experiment (MELT) region of the East Pacific Rise from analysis of P and S body waves. *J. Geophys. Res.* **108,** 2176 (2003).
48. Geist, D. J. *et al.* Submarine Fernandina: Magmatism at the leading edge of the Galápagos hot spot. *Geochem. Geophys. Geosyst.* **7,** Q12007 (2006).
49. Workman, R. K. & Hart, S. R. Major and trace element composition of the depleted MORB mantle (DMM). *Earth Planet. Sci. Lett.* **231,** 53–72 (2005).
50. Sun, S. S. & McDonough, W. F. Chemical and isotopic systematics of oceanic basalts: Implications for mantle composition and processes. *Geol. Soc. Lond. Spec. Pub.* **42,** 313–345 (1989).

Acknowledgements

We thank Minard Hall of the Instituto Geofísico of the Escuela Politécnica Nacional in Quito, the Charles Darwin Research Station, and the Parque Nacional Galápagos for logistical support and assistance in the field. M. Jackson provided constructive comments that improved this paper. This research was supported by the National Science Foundation under grants OCE-9908695, OCE-0221549, and EAR-0651123 to the University of Oregon, OCE-0221634 to the Carnegie Institution of Washington, and EAR-11452711 to the University of Idaho.

Author contributions

D.R.V., D.R.T. and D.J.G. wrote the initial manuscript. D.R.V., D.R.T., E.E.E.H. and S.C.S. contributed to experiment design and collection of seismic data. D.R.V., D.R.T. and E.E.E.H. contributed to the analysis of seismic data and methods development. D.J.G. contributed to the petrologic calculations and to the development of geochemical models. All authors discussed the results and their implications and assisted in the final revisions to the manuscript.

Additional information

Supplementary information is available in the online version of the paper. Reprints and permissions information is available online at www.nature.com/reprints. Correspondence and requests for materials should be addressed to D.R.T.

Competing financial interests

The authors declare no competing financial interests.